Papers in Natural Resources   Natural Resources, School of

2022

Influence of irrigation on diurnal mesoscale circulations: results from GRAINEX

C. Phillips

R. Mahmood
University of Nebraska - Lincoln, rmahmood2@unl.edu

R. Pielke Sr.

Geophysical Research Letters®

Key Points:

- First extensive observational study of modification of slope wind circulations by irrigation
- Presence of irrigation in upslope regions weakens terrain-induced baroclinicity
- Irrigation-reduced baroclinicity weakens the afternoon slope wind circulation

Supporting Information:

Supporting Information may be found in the online version of this article.

Correspondence to:

U. S. Nair,
nairu@uah.edu

Author Contributions:

Conceptualization: C. E. Phillips, U. S. Nair
Formal analysis: C. E. Phillips, U. S. Nair
Funding acquisition: U. S. Nair, R. Mahmood, E. Rappin, R. A. Pielke
Investigation: C. E. Phillips, U. S. Nair
Methodology: C. E. Phillips, U. S. Nair
Project Administration: U. S. Nair, R. Mahmood, E. Rappin, R. A. Pielke
Software: C. E. Phillips
Validation: C. E. Phillips, R. Mahmood
Visualization: C. E. Phillips
Writing – original draft: C. E. Phillips
Writing – review & editing: C. E. Phillips, U. S. Nair, R. Mahmood, E. Rappin, R. A. Pielke

Influence of Irrigation on Diurnal Mesoscale Circulations: Results From GRAINEX

C. E. Phillips[1], **U. S. Nair[1]**, **R. Mahmood[2]**, **E. Rappin[3]**, and **R. A. Pielke Sr[4,5]**

[1]Atmospheric and Earth Science Department, University of Alabama in Huntsville, Huntsville, AL, USA, [2]High Plains Regional Climate Center, School of Natural Resources, University of Nebraska-Lincoln, Lincoln, NE, USA, [3]Kentucky Climate Center, Western Kentucky University, Bowling Green, KY, USA, [4]Department of Atmospheric and Oceanic Sciences, University of Colorado Boulder, Boulder, CO, USA, [5]Cooperative Institute for Research in Environmental Sciences, University of Colorado Boulder, Boulder, CO, USA

Abstract In order to understand the impact of irrigation on weather and climate, the 2018 Great Plains Irrigation Experiment collected comprehensive observations straddling irrigated and non-irrigated regions in southeast Nebraska. Using these observations, we examine how irrigation affects diurnal terrain-generated slope circulations, specifically the slope wind. We find that irrigation applied to upslope regions of gently sloping terrain reduces terrain-induced baroclinicity and the associated pressure gradient force by up to two-thirds. This leads to the reduction in the afternoon and evening upslope wind and is supported through comparisons to the High-Resolution Rapid Refresh operational model, which does not explicitly account for irrigation. Additionally, the presence of irrigation decreases daytime sensible heat flux (Bowen ratio reduced 40% compared to non-irrigated regions), weakening turbulent transport of momentum. Modifications to the terrain-forced circulation by irrigation has the potential to affect moisture transport and thus cloud and precipitation formation over the Great Plains.

Plain Language Summary Agricultural irrigation alters input of heat and moisture from the land surface to the atmosphere, which can affect weather and climate. Irrigation is expanding on all continents except Antarctica and is thus a major pathway through which humans impact the environment. However, the observations required to study the mechanisms though which irrigation affects weather and climate are lacking. The Great Plains Irrigation Experiment (GRAINEX) was conducted to collect such observations near the boundary between irrigated and non-irrigated regions in southeast Nebraska. During the daytime, the slope of the Great Plains causes near-surface upslope winds and downslope winds in the atmosphere above. At night this pattern reverses. This wind system influences storm formation by forcing upward motion and transporting moisture. Using the observations from GRAINEX and comparing to a weather model we find that irrigation weakens this wind system, potentially affecting cloud and rain formation in this region.

1. Introduction

In the modern agricultural economy, irrigation is a crucial practice that increases crop yields and extends arable land into semi-arid and arid regions (Zohaib & Choi, 2020). While globally only 20% of farmland is irrigated, such regions account for 40% of food production (Decker et al., 2017). Further, irrigation represents the largest burden on the fresh water supply, being over 70% of annual demand (Cai & Rosegrant, 2002), and is expected to expand on every continent except Antarctica (Zohaib & Choi, 2020). Irrigation substantially modifies all aspects of the hydrologic cycle including soil moisture, precipitation, and surface moisture fluxes (Huber et al., 2014; Kang & Eltahir, 2019; Sridhar, 2013; Yang et al., 2019). The atmospheric responses to irrigation, however, are complex and vary in both time and space (Cook et al., 2011; D. Lobell et al., 2009).

Much work has been devoted to understanding the atmosphere's response to widespread irrigation, and the topic remains an area of active research. Irrigation modifies soil moisture both locally and remotely through precipitation downwind of the irrigated region (Barnston & Schikedanz, 1984; Deangelis et al., 2010; Kang & Eltahir, 2019; Lawston et al., 2017; Moore & Rojstaczer, 2002; Nauert & Ancell, 2019; Niyogi et al., 2010). Moreover, irrigation reduces the Bowen ratio (the ratio of sensible to latent heat flux), producing additional atmospheric responses that include: reducing daytime surface temperature and increasing nighttime temperature (D. B. Lobell & Bonfils, 2008; Qian et al., 2013; Sorooshian et al., 2011; Sridhar, 2013; Yang et al., 2019),
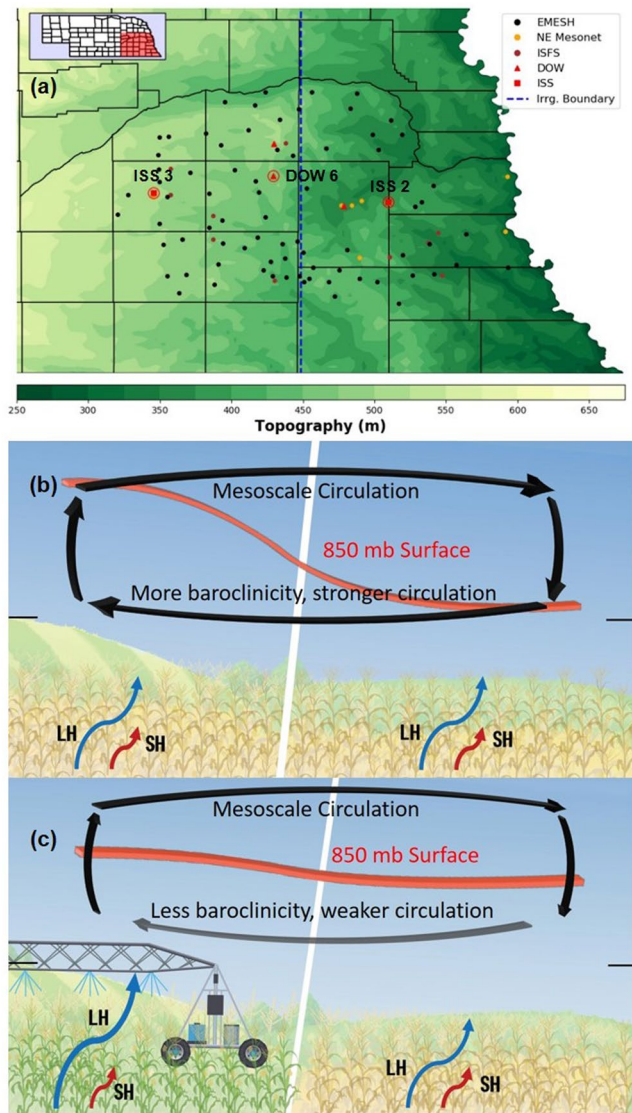
Figure 1. (a) The Great Plains Irrigation Experiment domain with topography shaded. Most irrigation within the study area is located west of 96.9°W (dashed line). Observation sites with rawinsondes are marked in red. Integrated Sounding Systems (ISS) 2, ISS 3 and Doppler on Wheels 6 are circled. ISS stations are separated by ~100 km. (b) Terrain-generated slope wind circulation in non-irrigated conditions. Red line is the 850 mb pressure surface, tilted by differential heating along the slope. Black arrows indicate the resulting circulation. Latent heat flux is denoted by the blue arrow, while sensible heat flux is in red. Black ticks show height of upslope region. (c) Same as (d) but with irrigation upslope. Irrigation reduces along-slope baroclinicity, weakening the circulation, which is illustrated by the gray arrow.

increasing atmospheric pressure (Kang & Eltahir, 2019), and modifying planetary boundary layer (PBL) and regional wind fields (Fast & McCorcle, 1991; Huber et al., 2014; McPherson, 2007; Ookouchi et al., 1984; Yang et al., 2020). Irrigation has also been found to increase the number and longevity of Great Plains' mesoscale convective systems (Qian et al., 2020) and increase convective available potential energy (Huber et al., 2014; Rappin et al., 2021; Yang et al., 2017). The strength and sign of these responses vary widely depending on the degree to which the surface energy budget is water or energy limited prior to the onset of irrigation (Cook et al., 2011).

One type of PBL circulation that may be modified by irrigation is the Great Plains slope wind. These winds are a diurnal mesoscale circulation that form due to differential atmospheric heating caused by the east-west slope of the Great Plains (Holton, 1967; McNider & Pielke, 1981). During the day, surface heating produces greater column warming in higher elevation (upslope) regions due to enhanced convergence of sensible heat flux. This produces a positive pressure perturbation and downslope winds aloft. Within the PBL, a compensating upslope wind forms. This process is reversed in the nocturnal PBL (McNider & Pielke, 1981, 1984).

The Great Plains slope wind and its associated baroclinicity and boundary layer structure are known to be factors in the formation and evolution of the Great Plains low-level jet (LLJ; Campbell et al., 2019; Gebauer & Shapiro, 2019; Holton, 1967; Lemone et al., 2014; Parish, 2017; Poulos et al., 2002; J. Sun et al., 2016). Additionally, convergence associated with mesoscale circulations influences convective initiation (CI; Barthlott et al., 2006). As the LLJ and CI both contribute to the rainfall distribution of the Great Plains, the slope wind is an important factor for regional climate. Baroclinic circulations like the slope wind also transport pollutants, which may have social and environmental consequences. The intensity of the slope wind, however, depends substantially on surface baroclinicity and PBL thermodynamic structure (De Wekker & Kossmann, 2015; Souza et al., 2000). Thus, irrigation may modify the climate of the Great Plains and similar regions with significant baroclinic circulations (conceptualized in Figure 1).

Despite considerable work by previous studies, there remain gaps in understanding the interactions between irrigation and mesoscale circulations such as the slope wind. Most studies that address the effects of irrigation (and soil moisture) on mesoscale circulations are theoretical in nature or utilize relatively coarse analysis grids that often poorly represent mesoscale phenomena (e.g., Anthes, 1984; Arcand et al., 2019; Campbell et al., 2019; Huber et al., 2014; Kueppers & Snyder, 2012; Ookouchi et al., 1984; Yang et al., 2020). This paper proposes to fill this gap using the extensive rawinsonde observations collected during the 2018 Great Plains Experiment (GRAINEX; Rappin et al., 2021) in Nebraska to characterize the impacts of irrigation on the Great Plains diurnal slope wind. Specifically, this paper seeks to:

1. Characterize the Great Plains slope wind before and after the onset of irrigation
2. Understand the impacts of irrigation on thermodynamic structure of the PBL and surface baroclinicity, and
3. Attribute modification of the Great Plains slope wind to irrigation

The remainder of this paper is organized as follows: the datasets and methodologies used during the study are presented in Section 2; the results are in Section 3; and the implications and conclusions of the work are in Section 4.

2. Methodology

Observations collected during GRAINEX, conducted during the growing season of 2018 in southeast Nebraska (Figure 1), are used to isolate the slope circulations and investigate how they are modified by irrigation. GRAINEX consisted of two Intensive Operation Periods (IOPs): 29th May-16th June 2018 (IOP 1) and July 17th-30th, 2018 (IOP 2) with reduced observations between those periods (Rappin et al., 2021). IOP 1 corresponds to the early growing period, when irrigation is limited, and IOP 2 occurs during the mid-growing season, which is characterized by vigorous crop growth and substantial irrigation. The GRAINEX domain (∼100 × 100 km) straddles the boundary between irrigated and non-irrigated croplands with irrigation being dominant west of longitude 96.9°W (Figure S1 in Supporting Information S1; Xie et al., 2021).

To characterize strong land and atmospheric gradients induced by irrigation, an extensive observation network was deployed, including rawinsondes from 5 locations launched bi-hourly beginning at dawn (0500 Local Standard Time [LST], 1100 Coordinated Universal Time [UTC]) and ending at dusk (1900 LST, 0100 UTC) during both IOPs. Additionally, 12 Integrated Surface Flux System (ISFS) stations (see Text S1 in Supporting Information S1), 2 Integrated Sounding Systems (ISS), 3 Doppler on Wheels (DOW), and 75 mesonet stations were deployed (Rappin et al., 2021). This study focuses on the analysis of rawinsondes released approximately along a west-east transect that includes ISS 2 (eastern site), DOW 6 (central site), and ISS 3 (western site). Note that these rawinsondes sample atmospheric conditions affected by land surface heterogeneity due to both gently sloping terrain and time varying irrigation effects in the western half of the transect, similar to prior studies (de Foy et al., 2005; Nair et al., 2011; Souza et al., 2000). DOWs 7 and 8 are not included in this analysis as they lie outside the west-east transect. While suitably cloudless days are limited, we additionally use a numerical experiment to supplement our observational analysis. Surface energy fluxes from ISFS stations are used to characterize land-atmosphere interactions under the effects of irrigation.

Similar to prior baroclinic circulation studies (e.g., Souza et al., 2000), circulations induced by land surface heterogeneity (terrain & irrigation) are isolated by negating daily averages of horizontal wind components as a function of altitude from corresponding bi-hourly rawinsonde observations. Mathematically:

$$u(z,t)' = u(z,t) - \bar{u}(z); \quad v(z,t)' = v(z,t) - \bar{v}(z) \tag{1}$$

Where u is zonal wind, v is meridional wind, z is altitude, and t is time at a specific location. Overbar represents the daily average. The bi-hourly perturbation profiles are averaged at each site for a selected set of case days during each IOP. This procedure yields mean bi-hourly perturbation wind profiles for the three sites during each IOP. Perturbation wind speed is then computed from the perturbation wind components.

In the above-described decomposition, diurnal variation of the perturbation wind within the PBL is modulated by turbulent mixing of momentum and heat, while the mean wind profile is determined by the synoptic scale pressure gradient force (PGF; Blackadar, 1957; Souza et al., 2000; Van de Wiel et al., 2010). In order to compute the diurnally varying portion of the PGF, which is induced by differential heating along the transect, perturbation pressure is calculated for each sounding site as follows:

$$p(z,t)' = p(z,t) - \bar{p}(z) \tag{2}$$

where p is observed pressure and the bar and prime denote the daily mean and perturbation from that mean respectively. The diurnally varying perturbation PGF is then calculated using a centered difference over the domain:

$$PGF(z,t) = -\frac{1}{\rho} \frac{p'_{\text{east}}(z,t) - p'_{\text{west}}(z,t)}{\Delta x} \tag{3}$$

where east and west correspond to ISS 2 and 3 respectively and Δx is the distance between those stations (∼100 km). Since irrigation impacts baroclinicity through alteration of PBL temperature and moisture, average bi-hourly altitudinal profiles of virtual temperature (T_v) are also analyzed for the case days during each IOP.

In addition, we compare results from the above-described analysis to corresponding simulated fields from the 3 km grid-spacing High Resolution Rapid Refresh (HRRR) operational model analysis (Benjamin et al., 2016; Blaylock et al., 2017; Lee et al., 2019). The above-described wind and PGF decomposition are repeated for each

rawinsonde launch location using HRRR-simulated profiles at the closest grid point. Note, that while the HRRR analysis implicitly incorporates some effects of irrigation through assimilation of in-situ and remote sensing observations, explicit effects of enhanced soil moisture fluxes are not represented due to the lack of irrigation parameterization. That is, the HRRR serves as a non-irrigated control with which observations may be contrasted. Indeed, this is validated by comparison of ISFS sensible and latent heating observations to HRRR simulated values during IOPs 1 and 2 (Text S2 in Supporting Information S1). Thus, the differences in diurnal evolution of perturbation winds and PGF between observations and the HRRR analysis are used to evaluate the effects of irrigation on PBL circulations.

To minimize the impact of cloud cover on analysis, the selected set of case days for each IOP is limited to those with low cloud cover and similar shortwave radiative forcing based on Geostationary Operational Environmental Satellite (GOES) 16, ISFS, and HRRR data (5 days in IOP 1 and 4 days during IOP 2; Table S1 and Figure S2 in Supporting Information S1). Further, National Weather Service Advanced Hydrologic Prediction Service (AHPS) historical precipitation totals (Lawrence et al., 2003) show that rainfall in the irrigated and non-irrigated regions is similar (within one standard deviation) during both IOPs. Thus, the effects of irrigation are isolated from those of varying cloud cover and rainfall.

Finally, as case days in the observational study are somewhat limited, the case of 22 July 2018 is chosen for numerical experiments using the Weather Research and Forecasting (WRF) model with and without irrigation parameterization (Skamarock et al., 2008; Sridhar et al., 2002; X. Sun et al., 2017; Valmassoi et al., 2019). Base irrigation rate in the WRF model is 4 mm, and adjusted by irrigation fraction within each grid cell, according to 2001 Moderate Resolution Imaging Spectroradiometer irrigation fraction (Ozdogan & Gutman, 2008). A full description of these experiments is in Text S3 in Supporting Information S1. While the results of the numerical modeling study are not the focus of this work, they provide additional support for the proposed interpretation of the GRAINEX observations.

3. Results and Discussion

Because the focus of this study is modification of PBL circulations by irrigation, the following discussion is restricted to below 2,000 m above ground level (AGL). The dominant pattern of perturbation wind within the PBL during both IOPs is transition to downslope in the early morning before decelerating as the PBL grows during the day. In the afternoon and evening, the PBL perturbation wind reverses to become upslope. Analysis of perturbation density and perturbation vertical PGF indicate that hydrostatic balance is applicable (Text S4 in Supporting Information S1). Thus, the dominant factors that influence the diurnal evolution of the PBL perturbation winds are diurnal variation of the PGF and turbulent mixing of momentum.

While the general behavior of the perturbation winds are similar between the two IOPs, there are differences in intensity and local vertical structure. Early morning perturbation wind speeds (Figure 2) are typically greater during IOP 1 than IOP 2 (generally 3–4 m s^{-1} vs. 2 m s^{-1}) and have a much deeper maximum (~500 vs. ~200 m). This is consistent with the greater PGF during IOP 1 compared to IOP two (maximum of 4E−4 m s^{-2} vs. 2E−4 m s^{-2}) at 0500 LST (Figure 3). The orientation of the morning perturbation wind during IOP one is predominantly westerly during IOP 1, but in IOP 2 the perturbation wind below 1,000 m AGL backs with height, shifting from easterly near the surface to west-northwest at 1,000 m. Notably, the perturbation PGF is consistently westerly below 1,500 m AGL during both IOPs, suggesting that other processes are responsible for the turning of the dawn perturbation wind.

The above-described differences affect the evolution of two perturbation wind features that are present during the early morning (0500 LST; 1100 UTC) of both IOPs: MS1 and MS2 (here M denotes morning and S the surface during IOPs 1 and 2; Figure 2) and MA1 and MA2 (here A denotes atmosphere; Figure 2). The nature of these features depends on the wind profile that exists during the previous evening at the onset of PBL decoupling, and their evolution is governed by such nighttime processes as the inertial oscillation and differential cooling along the slope of the GRAINEX domain (Blackadar, 1957; McNider & Pielke, 1981; Shapiro & Fedorovich, 2009). In particular, McNider and Pielke (1981) used a two-dimensional model to show differential heating of a slope during daytime produces a mesoscale PGF that accelerates the wind after sunset. They also found nighttime radiative cooling along the slope reverses the slope temperature gradient, changing the sign of the thermal wind, and contributing to nighttime wind oscillations. Shapiro and Fedorovich (2009) developed a mathematical model that
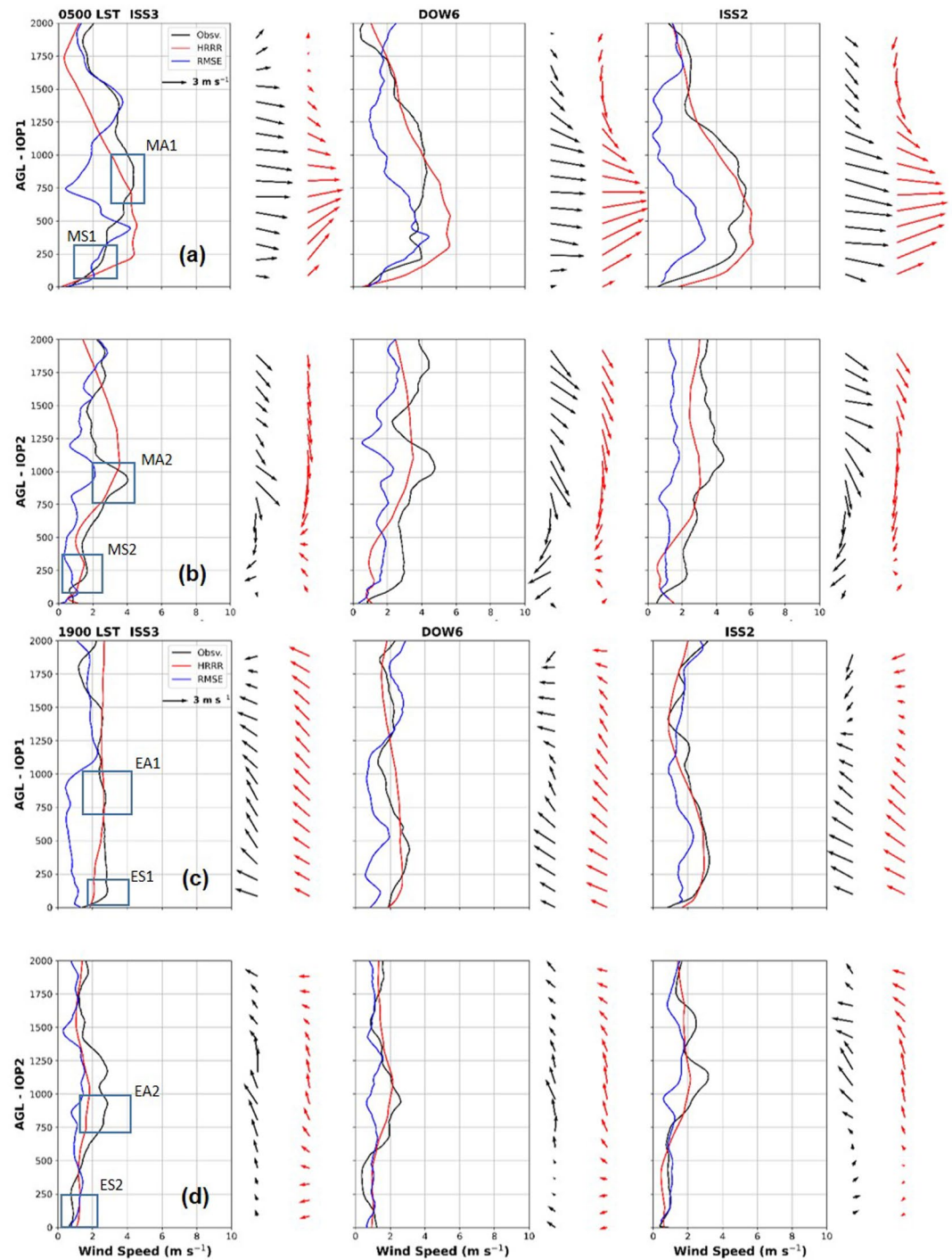
Figure 2. Composited perturbation wind speed for observations (black), the High Resolution Rapid Refresh (red), and the corresponding RMSE (blue) (a and b) are the wind profiles at local dawn (c and d) are the wind profiles at local sunset. Vectors indicate direction and scale with wind speed. Wind maxima of interest are boxed and labeled.

combines the Blackadar mechanism with an along-slope buoyancy gradient over sloped-terrain. In each study, these processes modified the PBL wind profile prior to morning over sloped terrain like the Great Plains.

During IOP 1, wind speed generally increases toward the east into the non-irrigated regions, but the shape of the wind profiles are similar in both irrigated and non-irrigated regions. The exception is MS1, which is only 2.5 m s^{-1} over ISS 3 and merges smoothly into MA1. Over ISS 2 MS1 is more distinct and is 5 m s^{-1}. In IOP
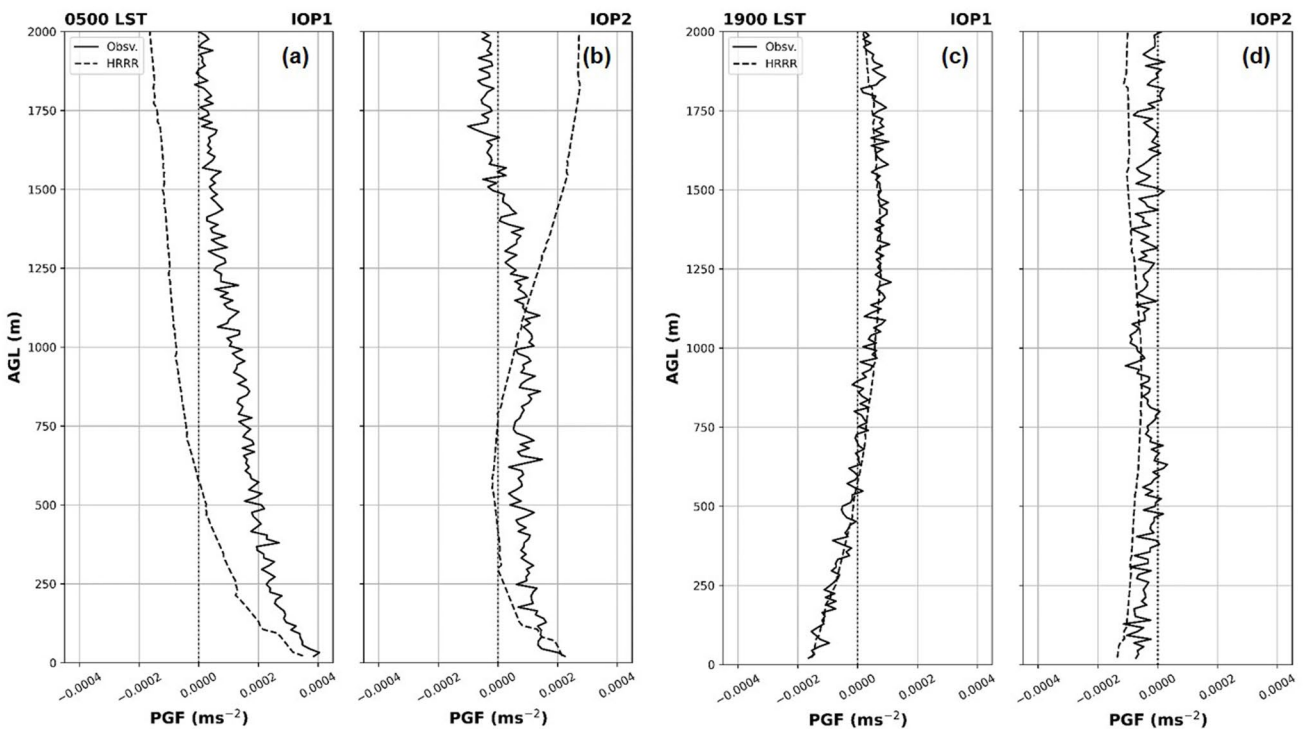
Figure 3. Zonal component of the perturbation pressure gradient force over the Great Plains Irrigation Experiment domain as calculated from the Integrated Sounding Systems rawinsondes (solid) and the High Resolution Rapid Refresh analysis (dashed) (left) Dawn and (right) sunset profiles are plotted for Intensive Operation Periods 1 and 2.

2, however, when the irrigation gradient appears, direction of MA2 differs between ISS 3 and ISS 2. There is a greater downslope component over the irrigated region than over the non-irrigated ISS 2 site.

The evening perturbation winds, ES1, ES2, EA1, and EA2 (where E denotes evening during IOPs 1 and 2; Figure 2), are dependent on the vertical mixing of momentum during the daytime and diurnal variation of the PGF and baroclinicity. The upslope perturbation winds at 1900 LST are stronger during IOP 1 due to both the enhanced zonal PGF (especially in the lower PBL at ES1 and ES2; Figure 3c) and vertical mixing of momentum. The greater vertical mixing during IOP one is driven by a combination of higher sensible heat flux (Figure S3 in Supporting Information S1) and reduced atmospheric stability (Figure 4). In fact, ISFS observations show a mean daytime Bowen ratio of 0.39 and 0.58 over the irrigated and non-irrigated areas respectively (Table S2 in Supporting Information S1), while the HRRR shows 0.42 and 0.77. The greater Bowen ratio in the model indicates that the HRRR is converting additional energy into sensible heating and consequent buoyant generation of turbulence. During IOP 2 turbulent mixing appears to a lesser degree with winds below 750 m AGL being less well-mixed over the irrigated ISS 3 site than the non-irrigated ISS 2 location.

Irrigation plays a role in reducing the magnitude of both the zonal PGF (Figure 3c) and vertical mixing of momentum during IOP 2. Higher soil moisture during IOP 2 produces shallower, but stronger nocturnal inversions compared to IOP 1 (Figures 4a and 4b). The reduced sensible heating over the irrigated upslope region (Table S3 in Supporting Information S1) reduces daytime differential heating along the slope, weakening generation of baroclinicity, which in turn weakens the PGF and subsequent slope wind circulation (Figure 1). Indeed, profiles of T_v differences across the GRAINEX domain indicate reduced diurnal variability of baroclinicity during IOP 2 (Figures S4a and S4c in Supporting Information S1). For example, above the surface layer, near 250 m AGL, T_v difference between the ISS 3 and ISS 2 sites ranges from approximately −1.9–1.8°C (nearly 4°C range) but this range decreases to approximately −1.3–0.5°C in IOP 2 (Figure S4a and S4c in Supporting Information S1). The reduced baroclinicity during IOP 2 continues until near 1,000 m AGL. By the equation of state, the temperature gradient across the GRAINEX domain effects the PGF. Thus, reduced baroclinic variability reduces the diurnal range of the PGF during IOP 2 (Figure 3). This combined with enhanced stability over irrigated regions, and
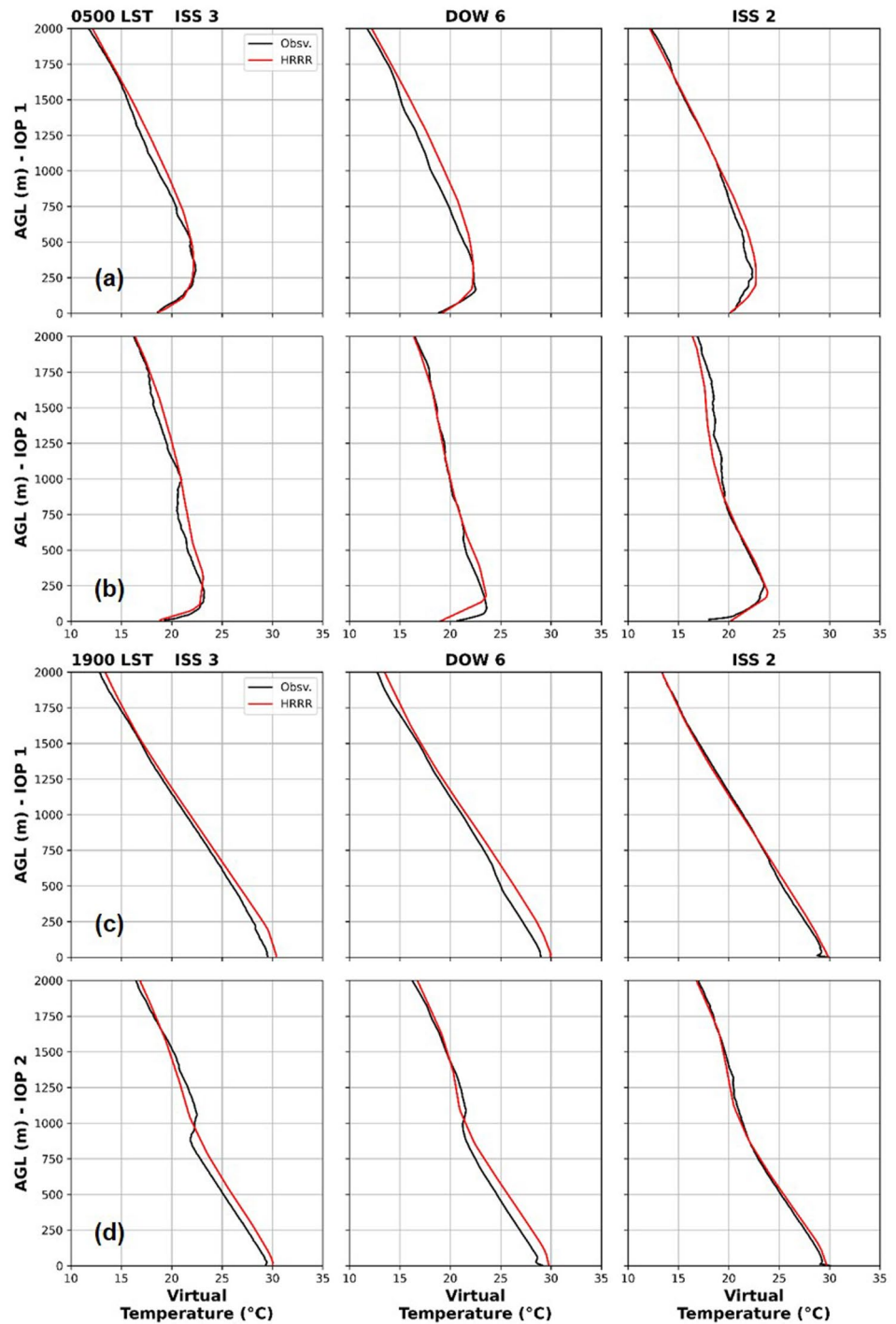
Figure 4. Composited virtual temperature for observations (black) and the High Resolution Rapid Refresh (red) for local dawn (a and b) and local sunset (c and d).

correspondingly weaker vertical mixing, produces weaker upslope winds in the late afternoon and evening hours when the PBL decouples. The ES1 upslope perturbation wind is nearly 3.0 m s^{-1} compared to ES2 which is less than 1.5 m s^{-1} and with almost no upslope component.

Overnight, these differing wind fields are subjected to the inertial oscillation (Blackadar, 1957; Shapiro et al., 2016; Van de Wiel et al., 2010), advection, and vertical mixing associated with shear-induced turbulence.

Thus, the behavior of the early morning near-surface slope flows (MS1 and MS2) and elevated jets associated with the remnant layer (MA1 and MA2) differ between IOP 1 and 2. Whereas features MS2 and MA2 appear as distinct local maxima in IOP 2, MS1 and MA1 nearly merge together. This could be due to the larger PGF at 1900 LST during IOP 1 in combination with it shifting from upslope to downslope with height (Figure 3c). This enhances vertical wind shear and shear-induced turbulence, mixing westerly momentum toward the surface overnight. Therefore, MS1 and MA1 are both westerly and blend together. During IOP 2, however, vertical variation of the perturbation PGF is reduced (Figure 3b), and early morning atmospheric stability is increased at both the surface and within the remnant layer (Figure 4), reducing vertical mixing of momentum and enabling MS2 and MA2 to evolve independently. These processes can explain why perturbation wind MS1 is 3–5 m s^{-1} downslope while perturbation wind MS2 is 2–3 m s^{-1} upslope depending on site (Figures 2a and 2b). MA1 and MA2 have similar magnitude (4–6 m s^{-1}) but have reduced depth during IOP 2 due to the reduced mixing. Additional work, however, is required to verify that these nocturnal processes are responsible for the observed differences in the morning wind profiles between IOPs.

When the above analysis is repeated using the HRRR analysis wind and thermodynamic fields, several differences emerge. These include the structure of the mixed-layer and perturbation winds, the diurnal variation of the PGF, and the strength of the residual layer inversion. Unlike the observational analysis, where MS1 and MA1 could be distinguished despite strong mixing, they cannot be readily identified as separate features in the HRRR analysis. Only one distinct jet maximum is apparent with a magnitude of 4–6 m s^{-1} downslope at 0500 LST during IOP 1. Additionally, the altitude of the jet maximum is 250–500 m lower than in the observational analysis (the greatest disparity is at DOW six in the center of the GRAINEX domain). As the HRRR analysis perturbation PGF shows good agreement with observations at 1900 LST (>2% error above 1,000 m AGL and below 250 m AGL), the time of PBL decoupling, other processes are likely responsible for the anomalous behavior of the HRRR morning wind profile. The tendency for HRRR to overestimate momentum mixing, especially within the nocturnal PBL (Fovell & Gallagher, 2020) could be responsible for the single jet feature. The HRRR analysis also shows more positive values of sensible heat flux overnight than observed, indicating the presence of enhanced nocturnal mixing (Figure S3 in Supporting Information S1).

During IOP 2, the 0500 LST perturbation wind profile shows differences between the HRRR and observations at all sites. While the tendency for wind to back with height is exhibited in both observations and the HRRR analysis, wind speed and direction differ. For example, MS2 and MA2 are underestimated by the HRRR analysis compared to observations (1.0–2.0 m s^{-1} vs. 2.0–3.0 m s^{-1} for MS2 and 3.0–3.5 m s^{-1} vs. 4.0–5.0 m s^{-1} for MA2; Figure 2). The discrepancies are greatest over DOW 6 and ISS 2, downslope of the irrigation. Further, MS2 and MA2 are northeasterly and southwesterly at all sites in observations, while the HRRR analysis shows southeasterly and northerly. At 1900 LST, during the time of PBL decoupling, the HRRR analysis over predicts the upslope intensity of ES2, even reversing the direction of the wind relative to observations over ISS 2. This is contrasted with IOP 1 where the HRRR simulated ES1 is in either fair agreement (DOW 6, ISS 2) or underestimated (ISS 3).

Comparison of the HRRR simulated fluxes to observations during IOP two (Figure S3c and S3d in Supporting Information S1) show that the HRRR overestimates sensible heat flux during the daytime (90 W m^{-2} excess during peak heating) and underestimates latent heat flux due to the lack of irrigation in the model. During IOP two ISFS observations show that irrigated regions have a mean daytime latent heat flux of 296 W m^{-2} compared to 175 W m^{-2} in the HRRR. Over non-irrigated regions, these values are 240 and 160 W m^{-2} respectively; thus, the HRRR underestimates mean daytime latent heat flux by −121 W m^{-2} over the irrigated sites but only by −74 W m^{-2} at the non-irrigated locations. This is in contrast to IOP 1 where HRRR overestimated latent heat flux in both regions by 57–59 W m^{-2} (Table S4 in Supporting Information S1), indicating that absent irrigation, the HRRR treats both regions similarly in terms of surface heat fluxes.

Further, the HRRR shows only an average 14% reduction in daytime mean sensible heat flux in irrigated regions compared to non-irrigated areas during IOP 2, but ISFS stations observed a 30% decrease (Table S3 in Supporting Information S1). For latent heat flux, ISFS observations show 23% increase in daytime latent heat flux compared to a 5% increase in the HRRR (Table S4 in Supporting Information S1). This is in contrast to IOP 1 where both observations and the HRRR show a 17% decrease in daytime mean sensible heat flux over the irrigated region relative to non-irrigated sites. IOP 1 daytime latent heat flux shows an increase of 27% and 22% in observations and the HRRR respectively compared to non-irrigated sites. Thus, when irrigation is active, the HRRR fails to capture the subsequent changes in surface heat flux. The enhanced sensible heating in the HRRR

compared to observations produces greater terrain-induced baroclinicity during the daytime and evening hours (~0.5°C below 1,000 m AGL; Figure S4c and S4d in Supporting Information S1) and a correspondingly larger PGF when the PBL decouples ($-1.5E-4$ m s^{-2} vs. $-1.0E-4$ m s^{-2}). This consequently affects lower-atmosphere T_v, perturbation PGF, the Great Plains slope wind, and operational forecasting thereof.

Discrepancies between the HRRR simulated and observed T_v profiles are noticeably greater over the irrigated ISS 3 site than the unirrigated ISS 2 site, leading to an underestimation of the remnant layer capping inversion at 1900 LST (Figures 4c and 4d). In fact, ISS3 average surface-850 hPa mean-layer T_v is 25.14°C across the observed case days at 1900 LST compared to 25.64°C in the HRRR. Over ISS 2 observations and the HRRR indicate 24.05°C and 24.29°C respectively. Thus, the T_v discrepancy between observations and HRRR is 0.25°C less than that over the irrigated ISS 3 site. This enables greater mixing of momentum within the HRRR model, broadening MA2 compared to observations (Figure 2).

By contrasting WRF simulations with and without irrigation, we determine the influence of irrigation on surface heat fluxes, perturbation PGF, and the Great Plains slope wind for the day of 22 July 2018 to supplement the observational analysis. In the irrigated regions, we find that daytime sensible heat flux decreases by -17.5 W m^{-2}, and latent heat flux increases by 4.6 W m^{-2} (Figure S5 in Supporting Information S1). In the non-irrigated regions, sensible heat and latent heat fluxes decrease by 0.1 and 1.1 W m^{-2} respectively. The decrease in sensible heat is consistent with prior irrigation modeling at the seasonal scale (Sridhar, 2013). Overall, trends in surface heat flux are similar compared to observations, but magnitudes differ.

As predicted in the conceptual model described in Figures 1b and 1c, when sensible heat in the model is preferentially decreased in irrigated regions, baroclinicity across the GRAINEX domain is decreased during the afternoon. This is quantified by the perturbation PGF which is reduced 10%–30% during the afternoon in the irrigated WRF compared to the non-irrigated (Figure S6c in Supporting Information S1). By 1900 LST, however, perturbation PGF is similar in both simulations below 1,000 m AGL but is greater in the irrigated simulation above 1,000 m AGL. In the morning though, perturbation PGF below 750 m AGL switches from 0.0001 m s^{-2} downslope to over 0.0002 m s^{-2} upslope when irrigation is turned on (Figure S6b in Supporting Information S1). A possible explanation is the presence of speed divergence over the GRAINEX domain. At 0700 LST, total wind speeds increase from a peak of less than 5 m s^{-1} near 250 m AGL over ISS 2–7.5 m s^{-1} over ISS 3 in the irrigated simulation and are oriented upslope (Figure S7 in Supporting Information S1). In the non-irrigated WRF, the total wind increases from less 5 m s^{-1} over ISS 2 to about 6.5 m s^{-1} over ISS 3. This divergence removes mass from the atmospheric column, reducing pressure in upslope regions. Wind speed over ISS 3 is potentially greater in the irrigated simulation due to reduced mixing within the PBL as seen in the observational analysis.

Resulting modifications to the dawn and evening perturbation wind are less pronounced than in the observational analysis and vary with location (Figure S8 in Supporting Information S1). Over irrigated regions, the 0500 LST wind between 250 and 750 m AGL has a greater downslope component than in the non-irrigated simulations. Over ISS 2 in the non-irrigation regions, however, perturbation wind in both simulations is similar. At 1900 LST, near dusk, the irrigated WRF shows perturbation winds below 750 m AGL with little-to-no along-slope component. The non-irrigated simulation shows slightly upslope flow below 250 m AGL and downslope winds at 500 m AGL over ISS 3. At ISS 2 in the east, the irrigated WRF shows enhanced downslope winds between 500 and 750 m AGL. Thus, the perturbation wind response to irrigation in WRF is complex and varies in space.

4. Conclusions

We utilize observations collected during the GRAINEX field campaign and numerical experiments to investigate the impacts of irrigation in upslope regions of gently sloping terrain. Our analysis shows that irrigation in upslope regions reduces terrain-induced differential heating with a corresponding weakening of the evening PGF prior to decoupling of the PBL. Comparison to HRRR analysis shows that, on average, the evening zonal component of the PGF within the PBL (below 1,000 m AGL) is overestimated by 100% when irrigation is not considered. Above the PBL, the zonal PGF is overestimated by 300% during the time of PBL decoupling. This is additionally supported by analysis using the WRF model, which shows a decrease in afternoon perturbation PGF and a complete reversal in the morning by irrigation. Due to weakening of along-slope baroclinicity, the evening near-surface upslope wind is nearly eliminated during IOP 2 when irrigation is prevalent compared to IOP 1 when the evening upslope wind approaches 3.0 m s^{-1}.

Further, irrigation observations from IOP 2 show that irrigated regions have 30% reduced daytime sensible heat flux compared to non-irrigated regions, while the operational HRRR model shows mean daytime sensible heat flux decreases only 14% relative to non-irrigated regions. Thus, irrigation reduces sensible heat flux, which helps stabilize the PBL and decreases momentum exchange between near-surface wind jets and those associated with the remnant layer inversion. This limits the depth of nocturnal jets that form over irrigated regions and reduces loss of momentum within elevated jets, increasing their strength relative to non-irrigated conditions. This contrasts with previous studies that find irrigation reduces the strength of nocturnal LLJs by reducing the along-slope temperature gradient (and subsequently the thermal wind) and reducing PBL mixing that creates an ageostrophic wind component (Campbell et al., 2019; Parish, 2017; Yang et al., 2020). Notably, past studies tend to focus on the southerly LLJ, but the jets in this work are zonal. Thus, the weakening of the along-slope temperature gradient and thermal wind are not as crucial to their development as in the southerly LLJ. Future work may wish to explore the differences in irrigation forcing on southerly LLJs compared to zonal ones in greater detail.

Our findings show that irrigation impacts the Great Plains slope wind through two primary processes: (a) decrease in baroclinicity reduces along-slope PGF, weakening or even eliminating the evening near-surface slope wind and (b) stabilization of the PBL reduces vertical transport of momentum, narrowing nocturnal jets. These results are consistent with prior modeling studies and to the best of our knowledge are the first observational confirmation of this effect. Since the vertical profile of horizontal winds at the time of PBL decoupling evolve overnight due to inertial oscillations, vertical mixing of momentum, and differential advection, irrigation also affects near-surface and remnant layer jets. Higher stability within the nocturnal stable boundary layer over wetter soils and stronger remnant layer inversions over irrigated regions enable more independent evolution of these wind features.

Note, that while our study provides the first observational analysis of irrigation-induced boundary layer circulations, it does not allow for quantification of all relevant forcing factors. This can only be achieved through combination of observational and numerical modeling analysis, which we have begun in this study, but further work is necessary. Additional analysis also needs to be conducted to investigate if the changes in PBL circulation affects cloud and precipitation formation.

Conflict of Interest

The authors declare no conflicts of interest relevant to this study.

Data Availability Statement

CSWR sounding data are available at https://doi.org/10.17632/822csmdp5g.1. NCAR/EOL sounding data for the ISS 2 and ISS 3 sites are located at https://doi.org/10.5065/D6WH2NV0 and https://doi.org/10.26023/P0KD-873S-510V. ISFS flux data are accessible via https://doi.org/10.26023/WPSA-MFSD-MC12. HRRR analysis is available at https://doi.org/10.7278/S5JQ0Z5B. AHPS rainfall totals may be downloaded at https://water.weather.gov/precip/download.php. Data are processed using the Python programming language. The WRF 4.3 model is available via UCAR at https://github.com/wrf-model/WRF.

References

Anthes, R. A. (1984). Enhancement of convective precipitation by mesoscale variations in vegetative covering in semiarid regions. *Journal of Climate and Applied Meteorology*, *23*(4), 541–554. https://doi.org/10.1175/1520-0450(1984)023<0541:eocpbm>2.0.co;2

Arcand, S., Luo, L., Zhong, S., Pei, L., Bian, X., & Winkler, J. A. (2019). Modeled changes to the Great Plains low-level jet under a realistic irrigation application. *Atmospheric Science Letters*, *20*(3), 1–10. https://doi.org/10.1002/asl.888

Barnston, A. G., & Schikedanz, P. T. (1984). The effect of irrigation on warm season precipitation in the southern Great Plains. *Journal of Climate and Applied Meteorology*, *23*(6), 865–888. https://doi.org/10.1175/1520-0450(1984)023<0865:teoiow>2.0.co;2

Barthlott, C., Corsmeier, U., Meißner, C., Braun, F., & Kottmeier, C. (2006). The influence of mesoscale circulation systems on triggering convective cells over complex terrain. *Atmospheric Research*, *81*(2), 150–175. https://doi.org/10.1016/j.atmosres.2005.11.010

Benjamin, S. G., Weygandt, S. S., Brown, J. M., Hu, M., Alexander, C. R., Smirnova, T. G., et al. (2016). A North American hourly assimilation and model forecast cycle: The Rapid Refresh. *Monthly Weather Review*, *144*(4), 1669–1694. https://doi.org/10.1175/MWR-D-15-0242.1

Blackadar, A. K. (1957). Boundary layer wind maxima and their significance for the growth of nocturnal inversions. *Bulletin of the American Meteorological Society*, *38*(5), 283–290. https://doi.org/10.1175/1520-0477-38.5.283

Blaylock, B. K., Horel, J. D., & Liston, S. T. (2017). Cloud archiving and data mining of High-Resolution Rapid Refresh forecast model output. *Computers & Geosciences*, *109*, 43–50. https://doi.org/10.1016/j.cageo.2017.08.005

Cai, X., & Rosegrant, M. W. (2002). Global water demand and supply projections. *Water International*, *27*(2), 159–169. https://doi.org/10.1080/02508060208686989

Campbell, M. A., Ferguson, C. R., Burrows, D. A., Beauharnois, M., Xia, G., & Bosart, L. F. (2019). Diurnal effects of regional soil moisture anomalies on the Great Plains low-level jet. *Monthly Weather Review*, *147*(12), 4611–4631. https://doi.org/10.1175/MWR-D-19-0135.1

Cook, B. I., Puma, M. J., & Krakauer, N. Y. (2011). Irrigation induced surface cooling in the context of modern and increased greenhouse gas forcing. *Climate Dynamics*, *37*(11), 1587–1600. https://doi.org/10.1007/s00382-010-0932-x

Deangelis, A., Dominguez, F., Fan, Y., Robock, A., Kustu, M. D., & Robinson, D. (2010). Evidence of enhanced precipitation due to irrigation over the Great Plains of the United States. *Journal of Geophysical Research: Atmospheres*, *115*(15), 1–14. https://doi.org/10.1029/2010JD013892

Decker, M., Ma, S., & Pitman, A. (2017). Local land – Atmosphere feedbacks limit irrigation demand. *Environmental Research Letters*, *12*, 054003. https://doi.org/10.1088/1748-9326/aa65a6

de Foy, B., Caetano, E., Magaña, V., Zitácuaro, A., Cárdenas, B., Retama, A., et al. (2005). Mexico City basin wind circulation during the MCMA-2003 field campaign. *Atmospheric Chemistry and Physics*, *5*(8), 2267–2288. https://doi.org/10.5194/acp-5-2267-2005

De Wekker, S. F. J., & Kossmann, M. (2015). Convective boundary layer heights over mountainous terrain—a review of concepts. *Frontiers of Earth Science*, *3*(December), 1–22. https://doi.org/10.3389/feart.2015.00077

Fast, J. D., & McCorcle, M. D. (1991). The effect of heterogeneous soil moisture on a summer baroclinic circulation in the central United States. *Monthly Weather Review*, *119*, 2140–2167. https://doi.org/10.1175/1520-0493(1991)119<2140:teohsm>2.0.co;2

Fovell, R. G., & Gallagher, A. (2020). Boundary layer and surface verification of the High-Resolution Rapid Refresh, version 3. *Weather and Forecasting*, *35*(6), 2255–2278. https://doi.org/10.1175/WAF-D-20-0101.1

Gebauer, J. G., & Shapiro, A. (2019). Clarifying the baroclinic contribution to the Great Plains low-level jet frequency maximum. *Monthly Weather Review*, *147*(9), 3481–3493. https://doi.org/10.1175/MWR-D-19-0024.1

Holton, J. R. (1967). The diurnal boundary layer wind oscillation above sloping terrain. *Tellus*, *19*(2), 200–205. https://doi.org/10.3402/tellusa.v19i2.9766

Huber, D. B., Mechem, D. B., & Brunsell, N. A. (2014). The effects of Great Plains irrigation on the surface energy balance, regional circulation, and precipitation. *Climate*, *2*(2), 103–128. https://doi.org/10.3390/cli2020103

Kang, S., & Eltahir, E. A. B. (2019). Impact of irrigation on regional climate over Eastern China. *Geophysical Research Letters*, *46*(10), 5499–5505. https://doi.org/10.1029/2019GL082396

Kueppers, L. M., & Snyder, M. A. (2012). Influence of irrigated agriculture on diurnal surface energy and water fluxes, surface climate, and atmospheric circulation in California. *Climate Dynamics*, *38*(5), 1017–1029. https://doi.org/10.1007/s00382-011-1123-0

Lawrence, B. A., Shebsovich, M. I., Glaudemans, M. J., & Tilles, P. S. (2003). *Silver spring*. Retrieved from https://water.weather.gov/precip/archive/AMS_Paper_Feb_2003.pdf

Lawston, P. M., Santanello, J. A., & Kumar, S. V. (2017). Irrigation signals detected from SMAP soil moisture retrievals. *Geophysical Research Letters*, *44*(23), 11–860. https://doi.org/10.1002/2017GL075733

Lee, T. R., Buban, M., Turner, D. D., Meyers, T. P., & Baker, C. B. (2019). Evaluation of the High-Resolution Rapid Refresh (HRRR) model using near-surface meteorological and flux observations from northern Alabama. *Weather and Forecasting*, *34*(3), 635–663. https://doi.org/10.1175/WAF-D-18-0184.1

Lemone, M. A., Tewari, M., Chen, F., & Dudhia, J. (2014). Objectively determined fair-weather NBL features in ARW-WRF and their comparison to CASES-97 observations. *Monthly Weather Review*, *142*(8), 2709–2732. https://doi.org/10.1175/MWR-D-13-00358.1

Lobell, D., Bala, G., Mirin, A., Phillips, T., Maxwell, R., & Rotman, D. (2009). Regional differences in the influence of irrigation on climate. *Journal of Climate*, *22*(8), 2248–2255. https://doi.org/10.1175/2008JCLI2703.1

Lobell, D. B., & Bonfils, C. (2008). The effect of irrigation on regional temperatures: A spatial and temporal analysis of trends in California, 1934-2002. *Journal of Climate*, *21*(10), 2063–2071. https://doi.org/10.1175/2007JCLI1755.1

McNider, R. T., & Pielke, R. A. (1981). Diurnal boundary-layer development over sloping terrain (Wangara). *Journal of the Atmospheric Sciences*, *38*(10), 21982–22212. https://doi.org/10.1175/1520-0469(1981)038<2198:dbldos>2.0.co;2

McNider, R. T., & Pielke, R. A. (1984). Numerical simulation of slope and mountain flows. *Journal of Climate and Applied Meteorology*, *23*, 1441–1453. https://doi.org/10.1175/0733-3021-23.10.1441

McPherson, R. A. (2007). A review of vegetation-atmosphere interactions and their influences on mesoscale phenomena. *Progress in Physical Geography*, *31*(3), 261–285. https://doi.org/10.1177/0309133307079055

Moore, N., & Rojstaczer, S. (2002). Irrigation's influence on precipitation: Texas High Plains, U.S.A. *Geophysical Research Letters*, *29*(16), 22–14. https://doi.org/10.1029/2002gl014940

Nair, U. S., Wu, Y., Kala, J., Lyons, T. J., Pielke, R. A., & Hacker, J. M. (2011). The role of land use change on the development and evolution of the west coast trough, convective clouds, and precipitation in southwest Australia. *Journal of Geophysical Research*, *116*(7), D07103. https://doi.org/10.1029/2010JD014950

Nauert, C. J., & Ancell, B. C. (2019). Quantifying the effect of irrigation on nonlocal aspects of the atmosphere. *Journal of Geophysical Research: Atmospheres*, *124*(14), 7852–7867. https://doi.org/10.1029/2018JD029043

Niyogi, D., Kishtawal, C., Tripathi, S., & Govindaraju, R. S. (2010). Observational evidence that agricultural intensification and land use change may be reducing the Indian summer monsoon rainfall. *Water Resources Research*, *46*(3), 1–17. https://doi.org/10.1029/2008WR007082

Ookouchi, Y., Segal, M., Kessler, R. C., & Pielke, R. A. (1984). Evaluation of soil moisture effects on the generation and modification of mesoscale circulations. *Monthly Weather Review*, *112*(11), 2281–2292. https://doi.org/10.1175/1520-0493(1984)112<2281:eosmeo>2.0.co;2

Ozdogan, M., & Gutman, G. (2008). A new methodology to map irrigated areas using multi-temporal MODIS and ancillary data: An application example in the continental US. *Remote Sensing of Environment*, *112*(9), 3520–3537. https://doi.org/10.1016/j.rse.2008.04.010

Parish, T. R. (2017). On the forcing of the summertime Great Plains low-level jet. *Journal of the Atmospheric Sciences*, *74*(12), 3937–3953. https://doi.org/10.1175/JAS-D-17-0059.1

Poulos, G. S., Blumen, W., Fritts, D. C., Lundquist, J. K., Sun, J., Burns, S. P., et al. (2002). CASES-99: A comprehensive investigation of the stable nocturnal boundary layer. *Bulletin of the American Meteorological Society*, *83*(4), 5552–5581. https://doi.org/10.1175/1520-0477(2002)083<0555:caciot>2.3.co;2

Qian, Y., Huang, M., Yang, B., & Berg, L. K. (2013). A modeling study of irrigation effects on surface fluxes and land-air-cloud interactions in the southern Great Plains. *Journal of Hydrometeorology*, *14*(3), 700–721. https://doi.org/10.1175/JHM-D-12-0134.1

Qian, Y., Yang, Z., Feng, Z., Liu, Y., Gustafson, W. I., Berg, L. K., et al. (2020). Neglecting irrigation contributes to the simulated summertime warm-and-dry bias in the central United States. *Npj Climate and Atmospheric Science*, *3*(1), 1–10. https://doi.org/10.1038/s41612-020-00135-w

Rappin, E., Mahmood, R., Nair, U., Pielke, R. A., Brown, W., Oncley, S., et al. (2021). The Great Plains Irrigation Experiment (GRAINEX). *Bulletin of the American Meteorological Society*, *102*, E1756–E1785. https://doi.org/10.1175/bams-d-20-0041.1

Shapiro, A., & Fedorovich, E. (2009). Nocturnal low-level jet over a shallow slope. *Acta Geophysica*, *57*(4), 950–980. https://doi.org/10.2478/s11600-009-0026-5

Shapiro, A., Fedorovich, E., & Rahimi, S. (2016). A unified theory for the Great Plains nocturnal low-level jet. *Journal of the Atmospheric Sciences*, *73*(8), 3037–3057. https://doi.org/10.1175/JAS-D-15-0307.1

Skamarock, W. C., Klemp, J. B., Dudhi, J., Gill, D. O., Barker, D. M., Duda, M. G., et al. (2008). *A Description of the Advanced Research WRF Version 3*. NCAR Technical Note.

Sorooshian, S., Li, J., Hsu, K. L., & Gao, X. (2011). How significant is the impact of irrigation on the local hydroclimate in Californias Central Valley? Comparison of model results with ground and remote-sensing data. *Journal of Geophysical Research*, *116*(6), 1–11. https://doi.org/10.1029/2010JD014775

Souza, E. P., Rennó, N. O., & Silva Dias, M. A. F. (2000). Convective Circulations Induced by Surface Heterogeneities. *Journal of the Atmospheric Sciences*, *57*(17), 2915–2922. https://doi.org/10.1175/1520-0469(2000)057<2915:ccibsh>2.0.co;2

Sridhar, V. (2013). Tracking the influence of irrigation on land surface fluxes and boundary layer climatology. *Journal of Contemporary Water Rersearch and Education*, *152*, 79–93. https://doi.org/10.1111/j.1936-704x.2013.03170.x

Sridhar, V., Elliott, R. L., Chen, F., & Brotzge, J. A. (2002). Validation of the NOAH-OSU land surface model using surface flux measurements in Oklahoma. *Journal of Geophysical Research*, *107*, 4418. https://doi.org/10.1029/2001JD001306

Sun, J., Lenschow, D. H., LeMone, M. A., & Mahrt, L. (2016). The role of large-coherent-eddy transport in the atmospheric surface layer based on CASES-99 observations. *Boundary-Layer Meteorology*, *160*(1), 83–111. https://doi.org/10.1007/s10546-016-0134-0

Sun, X., Holmes, H. A., Osibanjo, O. O., Sun, Y., & Ivey, C. E. (2017). Evaluation of surface fluxes in the WRF model: Case study for farmland in rolling terrain. *Atmosphere*, *8*(10), 1–23. https://doi.org/10.3390/atmos8100197

Valmassoi, A., Dudhia, J., Di Sabatino, S., & Pilla, F. (2019). Evaluation of three new surface irrigation parameterizations in the WRF-ARW v3.8.1 model: The Po Valley (Italy) case study. *Geoscientific Model Development Discussions*, 1–33. https://doi.org/10.5194/gmd-2019-223

Van de Wiel, B. J. H., Moene, A. F., Steeneveld, G. J., Baas, P., Bosveld, F. C., & Holtslag, A. A. M. (2010). A conceptual view on inertial oscillations and nocturnal low-level jets. *Journal of the Atmospheric Sciences*, *67*(8), 2679–2689. https://doi.org/10.1175/2010JAS3289.1

Xie, Y., Gibbs, H., & Lark, T. (2021). Landsat-based Irrigation Dataset (LANID): 30-m resolution maps of irrigation distribution, frequency, and change for the U.S., 1997–2017. *Earth system science data discussions*, *13*(12), 5689–5710. https://doi.org/10.5194/essd-2021-207

Yang, Z., Dominguez, F., Zeng, X., Hu, H., Gupta, H., & Yang, B. (2017). Impact of irrigation over the California Central Valley on regional climate. *Journal of Hydrometeorology*, *18*(5), 1341–1357. https://doi.org/10.1175/JHM-D-16-0158.1

Yang, Z., Qian, Y., Liu, Y., Berg, L. K., Gustafson, W. I., Feng, Z., et al. (2020). Understanding irrigation impacts on low-level jets over the Great Plains. *Climate Dynamics*, *55*(3), 925–943. https://doi.org/10.1007/s00382-020-05301-7

Yang, Z., Qian, Y., Liu, Y., Berg, L. K., Hu, H., Dominguez, F., et al. (2019). Irrigation impact on water and energy cycle during dry years over the United States using convection-permitting WRF and a dynamical recycling model. *Journal of Geophysical Research: Atmospheres*, *124*(21), 11220–11241. https://doi.org/10.1029/2019JD030524

Zohaib, M., & Choi, M. (2020). Satellite-based global-scale irrigation water use and its contemporary trends. *The Science of the Total Environment*, *714*, 136719. https://doi.org/10.1016/j.scitotenv.2020.136719